

Article

Flow and Transport Numerical Model of a Coastal Aquifer Based on the Hydraulic Importance of a Dyke and Its Impact on Water Quality. Manglaralto—Ecuador

Paúl Carrión-Mero ^{1,2,*} , F. Javier Montalván ³ , Fernando Morante-Carballo ^{1,4,5} ,
Carolina Loor-Flores de Valgas ^{1,2} , Boris Apolo-Masache ^{1,2,*}  and Javier Heredia ⁶ 

- ¹ Centro de Investigaciones y Proyectos Aplicados a las Ciencias de la Tierra (CIPAT), ESPOL Polytechnic University, Campus Gustavo Galindo Km 30.5 Vía Perimetral, P.O. Box 09-01-5863, Guayaquil, Ecuador; fmorante@espol.edu.ec (F.M.-C.); mcloor@espol.edu.ec (C.L.-F.d.V.)
 - ² Facultad de Ingeniería en Ciencias de la Tierra, ESPOL Polytechnic University, Campus Gustavo Galindo Km 30.5 Vía Perimetral, P.O. Box 09-01-5863, Guayaquil, Ecuador
 - ³ Facultad de Ciencias de la Ingeniería, Centro de Investigación e Innovación de Geociencias (CIGEO), Universidad Estatal Península de Santa Elena (UPSE), Avda. Principal La Libertad-Santa Elena, La Libertad 240204, Ecuador; fmontalvan@upse.edu.ec
 - ⁴ Geo-Recursos y Aplicaciones GIGA, ESPOL Polytechnic University, Campus Gustavo Galindo Km 30.5 Vía Perimetral, P.O. Box 09-01-5863, Guayaquil, Ecuador
 - ⁵ Facultad de Ciencias Naturales y Matemáticas (FCNM), ESPOL Polytechnic University, Campus Gustavo Galindo Km. 30.5 Vía Perimetral, P.O. Box 09-01-5863, Guayaquil, Ecuador
 - ⁶ Instituto Geológico y Minero de España, Ríos Rosas, 23, 28003 Madrid, Spain; j.heredia@igme.es
- * Correspondence: pcarrion@espol.edu.ec (P.C.-M.); bhapolo@espol.edu.ec (B.A.-M.); Tel.: +593-998-265-290 (P.C.-M.); +593-98-564-1396 (B.A.-M.)



Citation: Carrión-Mero, P.; Montalván, F.J.; Morante-Carballo, F.; Loor-Flores de Valgas, C.; Apolo-Masache, B.; Heredia, J. Flow and Transport Numerical Model of a Coastal Aquifer Based on the Hydraulic Importance of a Dyke and Its Impact on Water Quality. Manglaralto—Ecuador. *Water* **2021**, *13*, 443. <https://doi.org/10.3390/w13040443>

Academic Editor: Nicolò Colombani
Received: 30 December 2020
Accepted: 2 February 2021
Published: 8 February 2021

Publisher's Note: MDPI stays neutral with regard to jurisdictional claims in published maps and institutional affiliations.



Copyright: © 2021 by the authors. Licensee MDPI, Basel, Switzerland. This article is an open access article distributed under the terms and conditions of the Creative Commons Attribution (CC BY) license (<https://creativecommons.org/licenses/by/4.0/>).

Abstract: Coastal aquifers are part of the natural resources contributing to local development and promote resilience in the most vulnerable communities near the sea. Manglaralto, an Ecuadorian coastal parish, is affected by water resource scarcity. The increase in salinity and deterioration of the water quality is generated by the local and floating population's demand, causing an increase in the Total Dissolved Solids (TDS) concentrations and decreasing the aquifer's piezometric levels. The aim is to establish a numerical model of flow and transport of the Manglaralto coastal aquifer by using hydrogeological data and Visual Transin software, relating the hydraulic importance of a dyke's design ("tape") and its impact on the quality of the water. The methodology is (i) hydrogeological database analysis, (ii) the system's recharge concerning the soil water balance, (iii) the boundary conditions of the flow and transport model and, (iv) the results and validation of the numerical simulation. The results configure the importance of the coastal aquifer's artificial recharge in the area where the tape is located, as reflected in the increase in piezometric levels and the decrease in salinity in wells near the sea. In conclusion, the numerical model of flow and transport allows expanding the knowledge of the variation of the piezometric levels and TDS concentrations over time, the importance of recharge in the hydrogeological system's operation, and correct community management resilience and projection to sustainable development.

Keywords: coastal aquifer; artificial recharge; seawater intrusion; flow and transport numerical model; dyke

1. Introduction

An aquifer is a natural reserve of freshwater corresponding to 1.7% of the Earth's total and about 30.1% of Earth's freshwater except for the Poles [1], a natural space that must be protected and monitored by several organizations. The wetlands convention (RAMSAR), one of the first global and environmental conventions adopted since 1971, its objective is the conservation of surface and groundwater hydrological systems for the protection of

ecosystems, guaranteeing the rational use of its resources, its importance, and international cooperation through its recognition and constant monitoring [2,3].

The recovery and management of wetlands must be examined according to their stress level and based on the various habitats that occur as alluvial plains, mangroves, arctic wetlands, marshes and forests [4]. They are promoting the increase of biodiversity, retaining surface water, and improving water and oxygen quality through appropriate recovery techniques in these habitats [4,5]. Contemplating its main geological and physical characteristics such as its ecosystem, geometry, water system and other characteristics highlight behavior and natural evolution [6]. For example, the RAMSAR wetlands of Andalucía—Spain, such as the Fuente de Piedra lagoon, Marismas del Odiel, lagoons of Cádiz, Albufera de Adra and other wetlands included in the RAMSAR list [7].

Groundwater is present in a lower proportion than surface water such as rivers and lakes but is considered as the engine of communities' economic and social development due to its use in homes, tourism development and, in general, for all human activity [8]. In Latin America, there are population settlements in coastal areas such as Argentina and Brazil. Therefore, this water resource's frequent use has generated some alteration in the water quality, encouraging the search for technical solutions and adequate management to improve its recovery and the areas' inhabitants' lives [9].

Some factors can alter aquifers, such as uncontrolled extraction by the entities in charge of their distribution, population increase, and even climate change [10,11]; the dissolution of soil materials due to precipitation and infiltration in the riverbed can cause an increase in salinity and the oxidation of pyrite in basal sands, such as the London basin aquifers [12]. In addition, the contaminants in interior aquifers (entering the continent) are caused by the influence of regional flows by other aquifers with high chloride concentration (as in the case of the Delhi area, which has 15 ppm to 5070 ppm) [13]. However, seawater's intrusion into coastal aquifers is influenced by the decrease in piezometric levels given the lack of rainfall or excess extraction, as in the case of the Mar del Plata—Argentina aquifer [14,15].

The groundwater of coastal aquifers around the world presents an annual depletion much higher than the recharge by precipitation and surface runoff, which is reflected in global hydrogeological models and neural networks [16,17], encouraging the search for methods and techniques that help in the recovery of the aquifer, promoting an artificial recharge that benefits the quality of the water and its advanced extraction [18,19]. Seawater intrusion has been another factor that influences aquifers. Various studies and designs of different numerical models are carried out, such as constant density, variable density, and solute transport, given the transition of fresh groundwater and seawater in regional aquifers [20].

The groundwater flow system is calculated by various methods. For example, in an aquifer system characterized by fractured rocks, the residence time can be calculated, obtaining a model based on the hydrochemistry of the water (using ions, which correctly discriminate the path of the water given its mineralogy), thus improving the management of this resource and its association with surface water in the area [21]. Several types of numerical models of variable density make it possible to relate or manage freshwater entry sources into coastal aquifers and their impact by the advance of seawater [22–24]. The SEAWAT-2000 numerical model is a coupled version of the model of flow (MODFLOW) and MT3DMS based on the finite difference method for this type of three-dimensional numerical simulation [25,26].

In Brazil, the model of flow (MODFLOW) and transport (MT3D) is implemented for the evaluation of aquifers and their current state in the face of pollution by wastewater in urban areas, thus achieving an optimistic forecast for the state of the aquifer and the quality of the water with proper management of polluting water and its streams [27,28]. In the “Salar de Atacama”—Chile, there are various groundwater recharge simulations and discharges using numerical models of the variable density and flow and transport models of constant density through the SHEMAT code, determining the importance of geochemical processes that alter the physical properties of an aquifer [29,30]. Pollution in

coastal aquifers due to seawater's advance is a complex process that can be analyzed using numerical models, such as the case of Querença-Silves in Portugal and Andhra Pradesh in India, where the hydraulic system's behavior and the correct management of the aquifer are highlighted [31,32].

The numerical models of flow and transport are used within scientific research to establish the hydraulic behavior in advance of seawater intrusion, validate the hypotheses raised in hydrogeological conceptual models, as well as the evolution in time of piezometric levels and concentrations of groundwater, for the proper management and planning of the water resources (in this case, coastal aquifers) necessary for the development of communities [33–35].

Santa Elena is a coastal province of Ecuador, recognized for its geological characteristics, mineral resources, historical geoscientific knowledge, and mainly for its tourist contribution to local development [36]. It has problems in distributing water to meet its communes' demand [37]. It has two primary sources of water; in the southern area, which corresponds to the urban part, the water resources are obtained through the Daule-Santa Elena diversion from the Guayas river basin, while, in the northern region, where the rural sectors are, it is supplied mainly from coastal aquifers [38].

In the Manglaralto parish, the primary source of water is underground, extracted from the coastal aquifer associated with the river of the same name [39], and in turn, it is considered a geosite of great relevance in the Geopark Project of the Santa Elena Peninsula [36]. The daily recharge occurs through the infiltration of surface water (rivers and streams that cross the limits of the aquifer), in addition to high-intensity rainfall in winter (December to May frequently) and small drizzles in June, July, and August. One of the difficulties present is the material that composes it, which is very porous and permeable, which causes the fast flow of groundwater to the sea. The Regional Administrative Board of Drinking Water of Manglaralto (JAAPMAN) is in charge of supplying the vital liquid to six communes (Figure 1), through 12 wells drilled. Although it is possible to supply most of the inhabitants, the rest of the population uses clandestine wells, “albarradas” (artisanal dams), tankers, and other sources [18]. For this reason, the scope of water in Manglaralto is limited and does not cover the necessary and economic activities of the area [39], identifying the sustainable management of the aquifer as a problem [40].

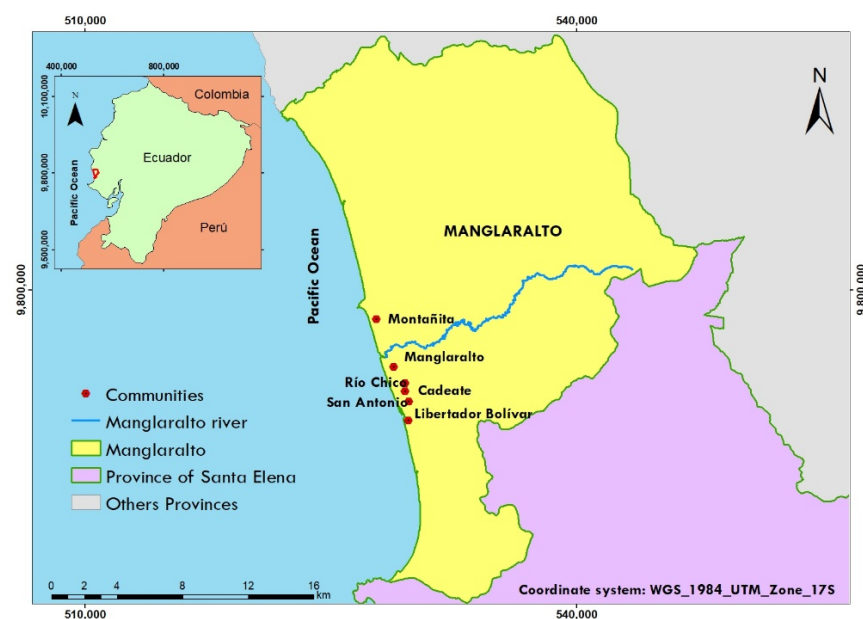


Figure 1. Location map of Manglaralto Parish.

Manglaralto has come to be considered a natural laboratory, given the community management for 40 years in the development, use, and protection of the aquifer and

academic and scientific participation, through various research projects and multiple undertakings about this resource. JAAPMAN is responsible for using groundwater and considers the management of wastewater with stabilization ponds and green filters for reforestation, using the soil as a natural filter in the commune of Montañita [41]. On the other hand, the issue of water and its management has recently been treated as an object of greater interest by many government researchers thanks to community participation, accompanied by ancestral knowledge, which have been key factors in solving problems regarding obtaining and distributing water, ensuring that the residents develop techniques to recharge the aquifer [18]. Within this participation, there are other significant parties involved, such as the International Atomic Energy Organization (IAEA) and the ESPOL Polytechnic University, which together with the community have managed to meet the growing water demand, rescuing ancestral knowledge by implementing tapes (artisanal dykes), addressing the overexploitation of the aquifer and empowering communities in water management [42]. However, in the geographical environment, problems remain due to tourism growth and climate change.

The main factors that affect and increase the water problem in the study area are marine currents and weather phenomena such as the warm El Niño current and the cold Humboldt current, which affect the intensity and regularity of rainfall [43,44]. In addition to having a semiarid climate [45], increased seawater intrusion is notoriously damaging water quality [38]. One of the solutions implemented is the rescue of ancestral knowledge with a technical-artisan tape [8] completed at the end of 2018. “Tape” is an ancestral-cultural term that the community members assign to the accumulation of rocks and sediments in certain strategic parts of the riverbed, damming the water or accumulate with the consequent artificial recharge aquifer [18]. By December 2019, it was evident how the coastal aquifer affected the communities’ socioeconomic development. The JAAPMAN provided the water service 24 h a day without interruption, positively influencing tourism in the sector, unlike in the past, where the service was only available at certain times.

As of March 2020, due to the global pandemic, another inevitable challenge is presented for Manglaralto, focused on overcoming the difficulties of proper water management. Studies carried out by [46] indicate that the groundwater system in Manglaralto is resilient where the community, despite global circumstances, has managed to adequately manage the water to avoid overexploitation of the aquifer without ruling out the household water. The aquifer is essential for these communities’ resilience in the face of the global crisis, even though it is an area affected by water scarcity related to climate change [18]. It has been possible to provide adequate hygiene, which is fundamental for each of the inhabitant’s very life and the resurgence of the coastal area, due to control and dedication by JAAPMAN towards its clients, despite the decrease in its leading economic resource, tourism [47].

The high demand problem due to socioeconomic relationships and climate change incidence by El Niño and La Niña leads us to ask ourselves the following question: is it possible to determine the advance of seawater intrusion by the influence of a tape on hydraulic behavior and groundwater density through a numerical flow and transport model?

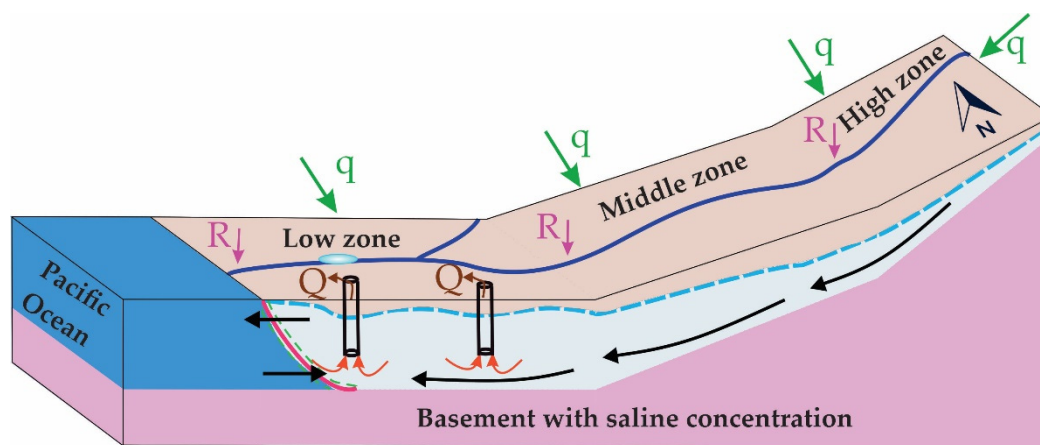
This research aims to establish a numerical model of flow and transport of the Manglaralto coastal aquifer, based on the conceptual model of the hydrogeological system, through the use of hydrogeological data and the application of Visual Transin software, relating the hydraulic importance of the design of a tape and its impact on water quality.

This analysis would help contribute to the resilience and sustainable development of the Manglaralto coastal aquifer. It will allow us to predict how the tape works and its importance in artificial recharge, positively affecting the biodiversity and geotourism of this Ecuadorian coastal zone.

2. Materials and Methods

The hydrogeological conceptual model encompasses all the specific data and scientific knowledge of the study site (Figure 2), managing to discretize the data domain and behavior

of the processes that influence water flow and the transport of solutes [48]. The water table in the middle and upper zones follows the geological survey guidelines carried out in the Manglaralto riverbed, indicating that in the middle zone, the average power of the aquifer is 10 m. In comparison, in the upper zone, the average power is 5 m. It is assumed that the water table is from 2 m below the level of the riverbed.



Simbology

- - - Water table
- - - Transition zone (H₂O aquifer-H₂O sea)
- Rivers
- Q Pumping
- ↻ Pumping flow
- Reservoir
- R Recharge
- q Lateral recharge
- Seawater income
- ← Groundwater discharge
- Wells
- ↶ Flow direction

Figure 2. Conceptual model of the hydrogeological system of the aquifer of the Manglaralto basin.

Before the methodological process that this investigative work entails, the vital work of the scientific information carried out in the study area must be considered. These data are stored using various works carried out by the community and academic institutions, such as geoelectric prospecting, workshops with the community, and recording the physical-chemical parameters and the static–dynamic levels of groundwater wells. These studies have a link with various projects (Table 1), such as:

Table 1. Projects related to the study area.

International Projects	Name
International Atomic Energy Agency (IAEA):	Characterization of Coastal Aquifers in the Santa Elena Peninsula-ECU/8/026
	Application of Isotopic Tools for Integrated Management of Coastal Aquifers-RLA/8/041
	Improving Knowledge of Groundwater Resources to Contribute to Their Protection, Integrates Management and Governance (CXXVII)-RLA 7/018
	Integrating Isotope Hydrology in National Comprehensive Water Resources Assessments-RLA 7/024
	Improvement of the Management of Coastal Aquifers by Studying the Recharge Rate of the Alluvial Aquifer of the Manglaralto River Basin-ECU/7/005
	Use of Isotopes for the Hydrogeological Evaluation of Excessively Exploited Aquifers in Latin America (CXXVII)-RLA/7/016

Table 1. Cont.

National Projects	Name
Social Link Project of Polytechnic University (ESPOL)	Hydrology and Hydrogeology Applied to the Coastal Aquifer of Manglaralto (Phase I, II, and III) -PG03-PY18-13
	Comprehensive Water Management in the Hydrogramic Basins of the Manglaralto Parish-PG03-PY19-09
	Resilience in Water Management, in the Face of COVID-19, Manglaralto-PG03-PY20-03
University of Santa Elena (UPSE)	Geophysical and Hydrochemical Characterization of the Manglaralto Aquifer for the Sustainability of the Water Resource-91870000.0000.382444

Darcy’s law governs the movement of underground flow in porous media [49]. The expressed conditions of variable density are in the supplementary material section.

The Visual Transin 4.0 and Transdens software solve the flow equation for a saturated and unsaturated zone, steady and transient, for transport, including a scattering-diffusion and advective process. The flow and transport equations can be developed decoupled (in constant density) or coupled (in variable density). These codes solve the flow and transport equations using finite elements in space and finite differences weighted in time.

This research work focuses on analyzing the scientific information and data collected from the study area, bearing in mind the zone’s geological and hydrogeological conditions, showing the reality of the coastal aquifer’s physical environment in a numerical model of flow and transport. A logical sequence is stipulated that starts from the conceptual model of the aquifer be studied. Subsequently, with the entire hydrogeological database and the zone’s hydrological cycle data, a soil water balance is carried out. It can be observed in the following methodological scheme, in the Figure 3.

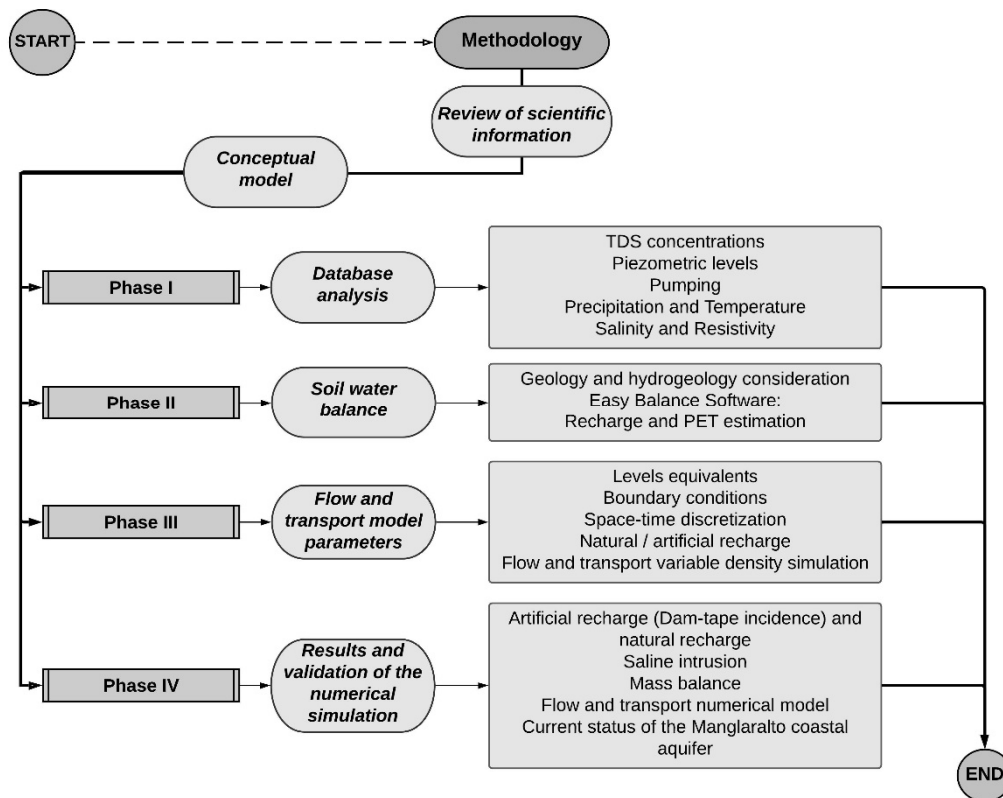


Figure 3. Scheme of the applied methodology.

2.1. Phase I

The compilation of information from the 11 study wells helps to ensure good order and technical formatting of the hydrogeological information (hydraulic, physical–chemical, and geological) managing to visualize in a general way the behavior of each well according to the month and year, and thus its direct relationship with piezometric levels, daily extraction, precipitations, and temperatures in the sector. These wells provide integrated hydrogeological information of the coastal aquifer, correlated with geology and geophysics, as shown in the conceptual model (Figure 2).

During this phase, the database of each well is analyzed. This information has been registered and reported monthly by JAAPMAN and the Center for Research and Projects Applied to Earth Sciences (CIPAT-ESPOL, acronym in Spanish), such as Total Dissolved Solids (TDS), salinity, temperature, resistivity, piezometric levels, and daily pumping extractions. The information on precipitation and temperature in the basin is from the Manglaralto meteorological station (Code: M0619).

2.2. Phase II

The Manglaralto coastal aquifer covers approximately 508 hectares and corresponds to 3.84% of the Manglaralto river basin in the surface territory. Permeable and porous materials predominate in this sector, identified as an alluvial terrace [50].

Figure 4 shows the geological formations that directly influence the alluvial aquifer, consisting mainly of gravel, sand, silt, and clay materials [38].

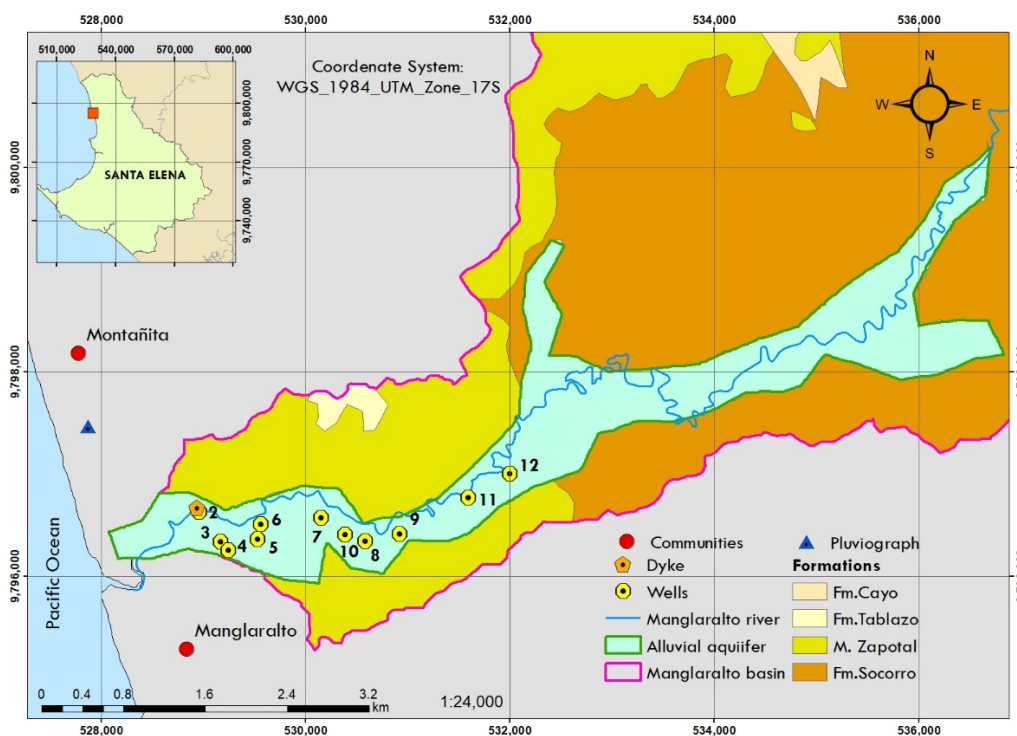


Figure 4. Geological map of the study area.

The formations are sequences of sedimentary and volcano–sedimentary rocks, and the ages range from the Upper Cretaceous to the Lower Miocene, followed by alluvial deposits from the Holocene [38].

This basement belongs to the Cayo Formation, which has powerful sequences of volcanic–sedimentary rocks. It is recognized for presenting graywacke sandstones and volcanic rocks a clay matrix, and gray or green silicified argillites, unlike the Tablazo Formation, where sequences of conglomerates and sands are evident. The Socorro Formation (Ancon Group) is stratigraphically like flysch with turbidites and thin layers of shales and

greenish sandstones [51]. The Zapotal Member that belongs to the Tosagua Formation contains significant amounts of chloride due to continuous contact with seawater and contains sandstone, conglomerates, and shales.

The transmissivity of the hydrogeological system is determined considering a theoretical permeability of 40 m/day (m/d), according to the gravel, sand, silt and clay materials present in the alluvial terrace, with an average saturated thickness of 20 m, 10 m for the middle zone and 5 m for the high zone.

In the soil–water balance, characteristic parameters such as field capacity, wilting point, precipitation, and temperature entered into the Easy Balance software were considered, estimating the aquifer recharge and Potential Evapotranspiration (PET). Recharge is a fundamental parameter in the simulation process, given its importance in the behavior of piezometric levels and water quality in these free and coastal aquifers.

It was essential for the field capacity and the wilting point to consider the clay soil according to its loamy texture, represented in volumetric content from percentage data and soil density [52,53]. Due to the presence of weeds in Manglaralto, it was possible to estimate a root thickness of 0.25 m and an initial humidity of 0. The design hyetograph of the Manglaralto basin indicates that the laminator value is 10 mm [54,55]

Finally, there is a useful reserve of 0 mm, and the initial reserve minor of 25 mm, used to calculate the PET and the recharge. Considering that the soil’s humidity and the vegetal layer are optimal, the information recorded on rainfall and temperatures from May 2018 to September 2020 is used through the Thornthwaite method to calculate the PET [56].

2.3. Phase III

Considering the basin’s hydrogeological system’s conceptualization, it could represent it through two layers; the upper layer corresponds to the aquifer, while the lower layer represents the basement (Figure 5). The first layer corresponds to the alluvial layer, classified into upper, middle, and lower, the latter strategically dividing into eight sub-zones according to the lateral recharge imposed on the model.

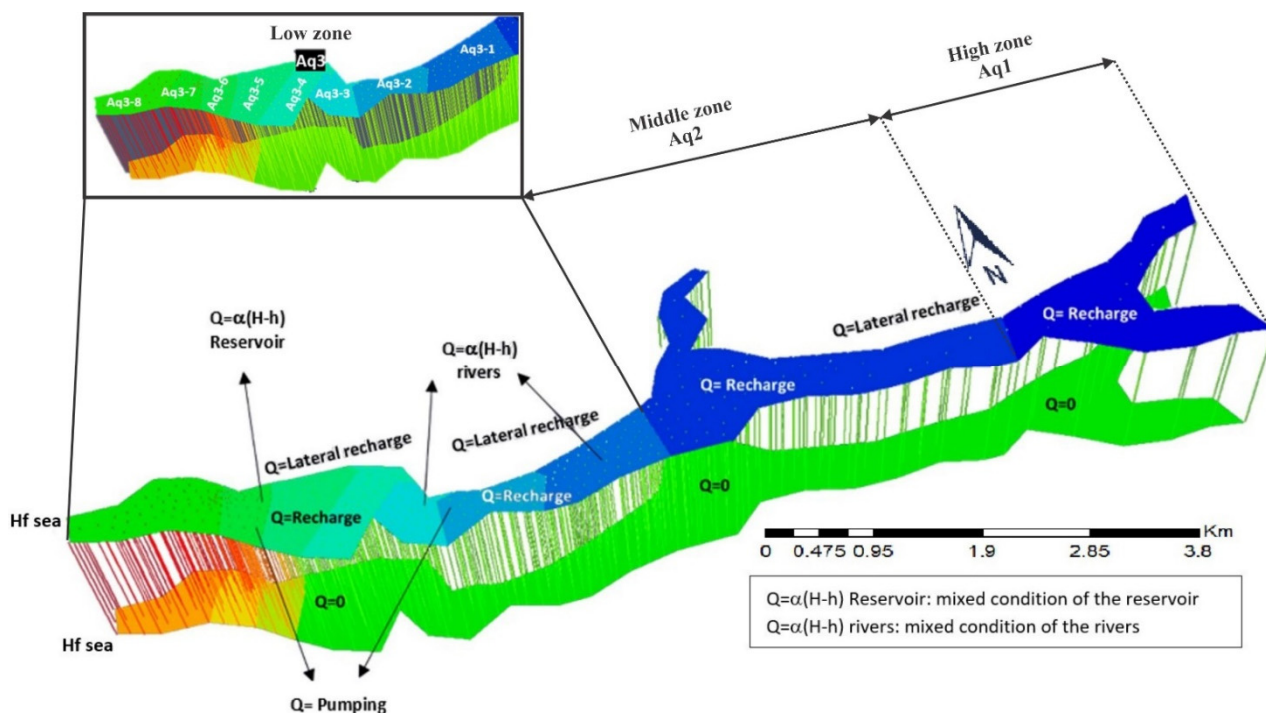


Figure 5. Boundary conditions for the flow model.

The transmissivities, the storage coefficient, porosity, and dispersivity of the aquifer correspond to the first layer’s three main zones. In the second layer (Figure 6), the aquifer’s

basement, in all its domain, presents a single zone of these parameters. In the basement, it is considered that there is no flow ($Q = 0$) because it is mainly made up of shale, silt and clay, for which a prescribed concentration condition is established.

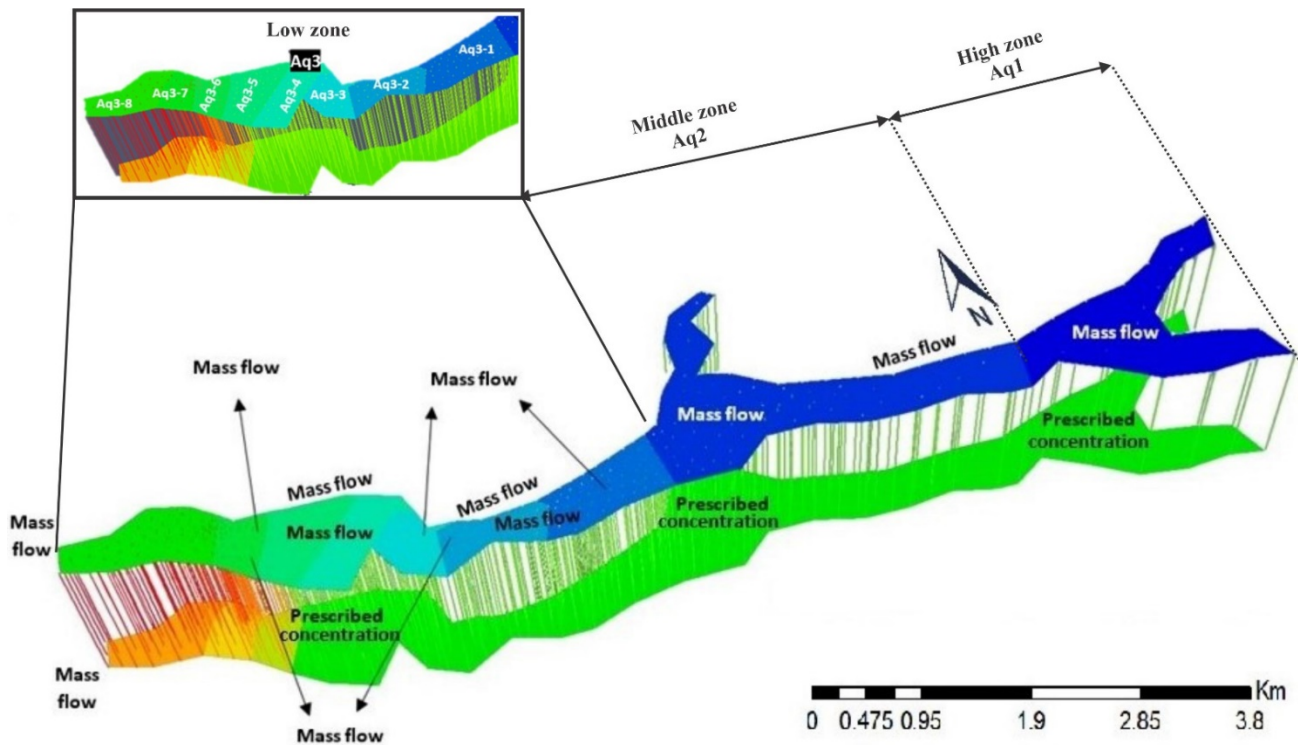


Figure 6. Boundary conditions for the transport model.

The recharge of the aquifer by rain infiltration is represented in a single zone corresponding to the alluvial one. Lateral recharge occurs around the aquifer’s edge, except in urbanized areas closest to the sea. The conditions of the flow and transport limits imposed on the model are in Tables 2 and 3.

Table 2. Boundary conditions of the flow problem.

Boundary Condition	First Layer	Second Layer
Prescribed level	Sea level Reservoir (tape) Rivers	Sea level
Prescribed flow	Pumping Lateral recharge	$Q = 0$
Mixed condition or Cauchy (leaked)	Reservoir (tape) Rivers	-

Table 3. Boundary conditions of the transport problem.

Boundary Condition	First Layer (Mass Flow)	Second Layer
External concentrations	Sea level Reservoir (tape) Rivers Lateral recharge Pumping	Sea level (mass flow) Basement (prescribed concentration)

The initial conditions used in the constant density model were the resolution of the first time step's flow and transport problem, since the model's numerical stability allowed it to go directly to the transitory model. This model was constructed prior to undertaking the variable density modelling.

The variable density model's initial conditions were the solution to the constant density flow and transport problem and by using the equivalent levels of fresh water in the constant and variable density models.

This work was carried out from 1 May 2018, to 30 September 2020; the simulation considered 29 months'-worth of data. It was possible to perform spatial discretization with a mesh of 952 nodes and 2068 elements. The largest mesh refining was carried out in the aquifer's lower area because it is an area of high hydraulic activity and groundwater discharge and is the sector where seawater enters.

2.4. Phase IV

In this section, the numerical model of flow and transport was obtained, that was subsequently analyzed to expand the knowledge of the aquifer piezometric levels and TDS concentrations, since this is related to the effect of the natural and artificial recharge produced by the water reservoir in the tape, its concentration in wells close to the sea due to marine intrusion and wells within the basin due to the saline basement's influence.

3. Results

The methodology used in this work provides the following results:

3.1. Soil Water Balance

Using Easy Balance 4.0 software, it was possible to obtain the soil–water balance; thus determining the PET and the recharge that enters the aquifer, using the simulation period's average monthly temperature.

March was the month with the highest PET (mm) in all years studied, with 200.16, 197.55, and 193.70 mm, respectively, in 2018, 2019 and 2020, (Table 4). The year with the highest value of this parameter is 2019 with 1596.95, while in 2020 until September, it is 1303.27 (Table 5); the PET in 2020 is higher compared to the years 2018 and 2019 in the same period.

Table 4. Maximum monthly values obtained in recharging and potential evapotranspiration (PET).

Year	Recharge [mm]			PET [mm]
	February	March	August	March
2018	5.6	-	7.3	200.16
2019	9.9	3.2	7.3	197.55
2020	3.8	-	-	193.70

Table 5. Annual data of the precipitations and values obtained in recharge and PET.

Year	Recharge [mm]	PET [mm]	Precipitation [mm]
2018	12.9	1584.89	127.3
2019	20.3	1596.95	213.4
2020	3.8	1303.27	38

Before estimating the recharge, the soil's characteristic parameters in the study basin needed for its determination were determined (Table 6). The recharge calculated for this period was 37 mm, which corresponds to 11.4% of the rainfall; in 2019, the recharge's highest value was 20.3 mm (Table 5). Table 4 shows the months that influenced the value of this recharge. It is essential to mention that in addition to the characteristics of the soil

(Table 6), the PET and rainfall influence recharge, especially in the months of February–March, which is when the highest rainfall occurs, while in July–August, low-intensity precipitations known as “garuas” (in Spanish) occur, which infiltrate the alluvial terrace and recharge the aquifer. The data and results of the PET and recharge estimation are in Table S1 of the complementary material.

Table 6. Estimation of soil characteristics.

Soil Characteristics	Value
Field capacity (volumetric content)	0.1
Initial humidity (volumetric content)	0
Soil root thickness (m)	0.25
Wilting point (volumetric content)	0.100
Rolling value (mm)	10

3.2. Mass Balance

The mass balance in the flow model in the transient regime and variable density conditions indicates that the inputs to the hydrogeological system are generated by recharge due to the infiltration of precipitation in the alluvial layer ($2.35 \text{ hm}^3/\text{y}$); lateral recharge at the edge of the aquifer ($32.21 \text{ hm}^3/\text{y}$); in the reservoir and the water network is represented by a mixed condition or leaked ($3.68 \text{ hm}^3/\text{y}$), and by a constant level that represents seawater entering the aquifer ($1 \text{ hm}^3/\text{y}$).

The outputs of the hydrogeological system are by pumping ($34.01 \text{ hm}^3/\text{y}$), in drainage in the highest aquifer area ($2.63 \text{ hm}^3/\text{y}$), and by the constant level that represents the aquifer discharge to the sea ($1.22 \text{ hm}^3/\text{y}$).

3.3. Numerical Model of Flow and Transport

3.3.1. Calibration

Regarding the calibration of the flow model, the following statistical parameters intervened: (i) on the mean absolute error (ϵ) of the piezometric levels, estimation of the sum of the absolute differences between the calculated levels (H_{cal}), and the number of total observations (H_{obs}), (ii) the Root Mean Square Error (RMSE), and (iii) the standard deviation. The mean absolute error was 0.0082, RMSE 0.12, and the standard deviation of 0.5.

The calibration strategy consisted of a manual stage based on trial and error criteria and an automatic one provided by the Visual Transin 4.0 software, which minimizes an objective function that it considers and the piezometric adjustment between measured and calculated values.

During this process, the zoning of the lower zone of the aquifer was modified due to inconsistencies in the reproduction of the measured levels, zoning it in eight subzones of transmissivity and storage coefficients in the first layer.

The piezometric adjustment between calculated and measured levels indicates that the calibration of the parameters presents a good fit, with a linear correlation coefficient (R^2) of 0.9818 (Figure 7), which indicates the robustness of the numerical representation due to the conditions contour of the natural zone.

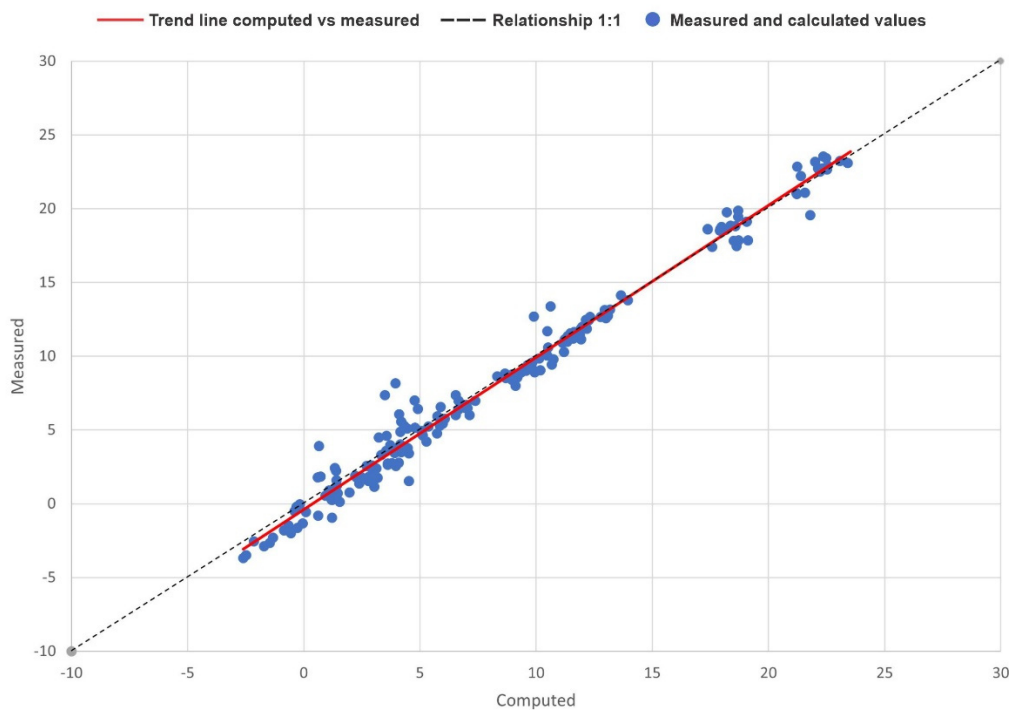


Figure 7. The statistical fit between measured and calculated levels.

The calibrated transmissivity and storage coefficient parameters in the flow model, both in constant and variable density, are shown in Table 7. The model’s calibration is based on statistical analysis with an adjustment of the piezometric levels measured in the field and those calculated in the simulation, obtaining values that are very close to each other, achieving an adjustment with reality.

Table 7. Calibrated parameters of transmissivity and storage coefficient of the flow model in constant and variable density.

Layers	Zones	Transmissivity (m ² /d)	Storage Coefficient	
		Value	Value	
Layer 1	High zone	Aq1	200	0.1
	Middle zone	Aq2	600	0.1
		Aq3-1	1000	0.1
	Low zone (Aq3)	Aq3-2	1000	0.1
		Aq3-3	1000	0.1
		Aq3-4	1000	0.1
		Aq3-5	1000	0.1
		Aq3-6	1000	0.2
		Aq3-7	2000	0.2
Layer 2	One zone for the whole domain	Aq3-8	1000	0.1
			0.00000001	0.2

In the transport model, the calibration was manual based on trial and error criteria. The calibration parameters were hydrodynamic dispersion and porosity, which remained constant at 0.2. These parameters were taken into account in the first and second layers since a saline concentration source was in the basement.

3.3.2. Lateral Recharge

The surface runoff from the rest of the basin is represented by recharging the aquifer’s edge, called lateral recharge. It is a significant water contribution to the system, being

estimated by Visual Transin 4.0, which considers the transmissivity, storage, and pumping parameters, the that fit the measured levels of the 11 wells used for this simulation.

The conceptualization of lateral recharge provided the simulation with calculated levels very close to those measured, approaching the reality of this hydrogeological system’s physical environment. The aquifer’s edge was divided into segments, highlighting that much of the data used is from the lower area due to the study wells’ locations.

3.3.3. Constant Density Flow Model

The aquifer’s upper zone is 5 m thick, while it is 10 m thick in the middle zone. The lower zone, where the porous and permeable aquifer materials’ greatest potency is, reaches thicknesses of approximately 30 m. The calibrated transmissivity and storage coefficient parameters indicate that the average permeability throughout the alluvial layer is approximately 40 m/d, with a storage coefficient of 0.2.

The calculated piezometric follows the measured piezometric. The model reproduces the hydraulic characteristics observed in the field (Figure 8). The wells closest to the sea generally have an excellent piezometric adjustment. However, during specific periods corresponding to the beginning of the 2019 rainfall season (wet), it is impossible to reproduce the observed piezometric in the wells P2 and P3, while the P4 presents the best fit. The wells inside the basins P5, P6, P7, P8, P9, and P10 present the present work’s best piezometric adjustment. In wells P11 and P12, the calculated versus measured piezometric levels are acceptable (Figure 8).

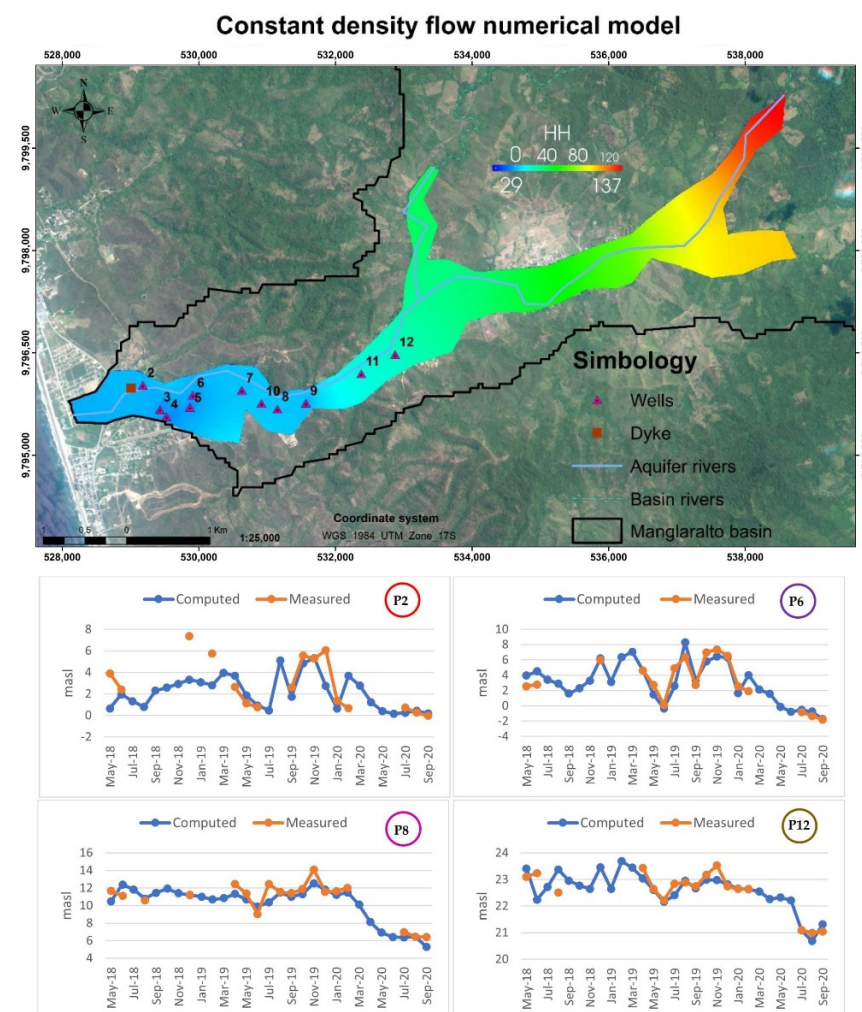


Figure 8. Constant density flow model and hydrograms of wells P2, P6, P8, and P12.

Transport Model

In well P2, the field concentrations show abrupt variations, going from 1000 mg/L to 6600 mg/L in one month, making the reproduction of these concentrations by Transden 2.0 complex. Wells P3, P4, P5, P6, and P7, present a reasonable adjustment in concentrations (TDS). Then the transport reproduces acceptably. In well P8 and P9, the calculated concentrations are below those measured, with a moderately acceptable fit. In wells P11 and P12, the calculated concentrations are above those measured, indicating that these wells have the highest saline concentration in the basin's interior because they are located very close to the middle zone, which has concentrations above 1500 mg/L in TDS (Figure 9).

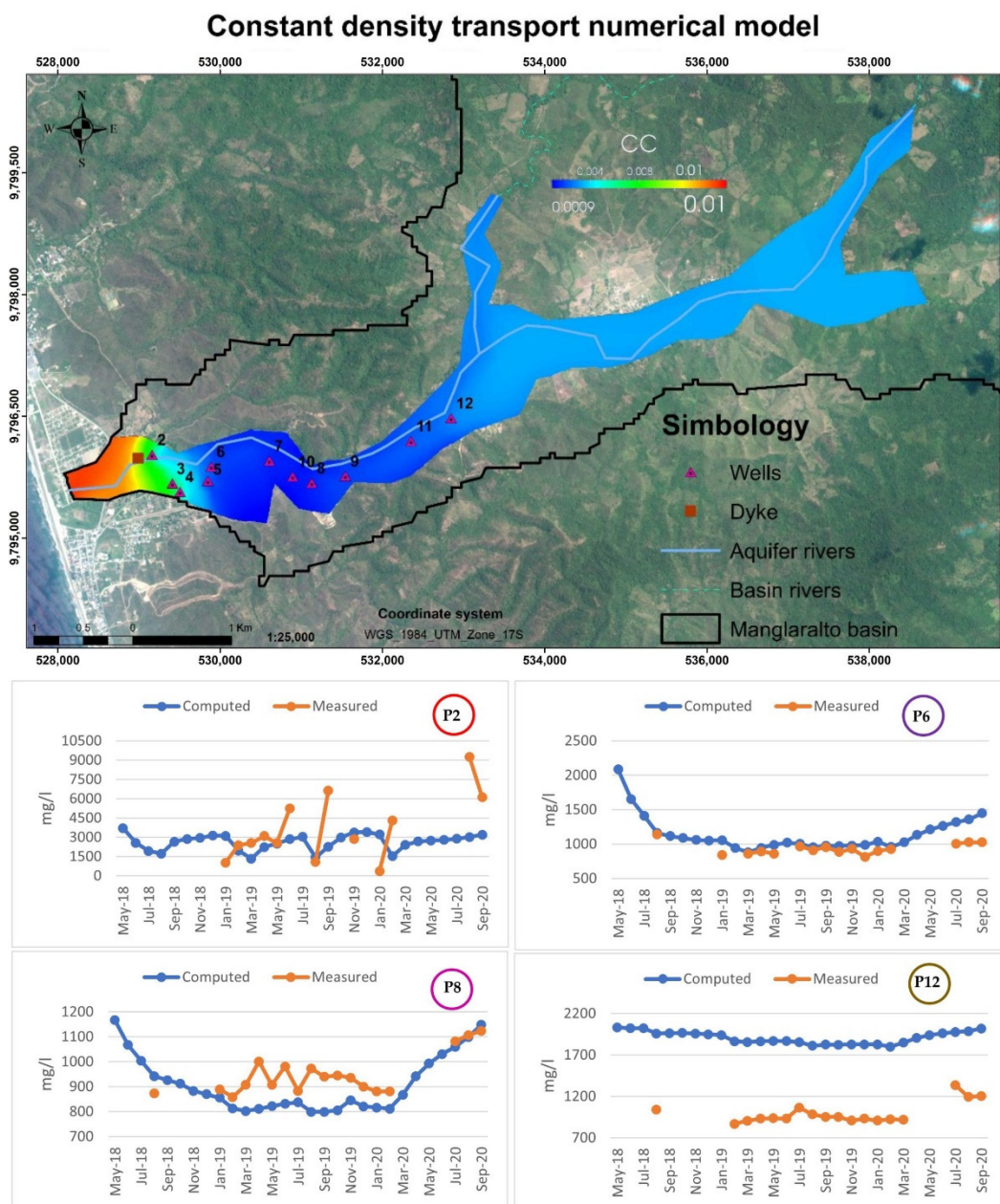


Figure 9. Transport model in constant density and hydrograms of wells P2, P6, P8, and P12.

3.3.4. Variable Density Flow Model

In all wells, except for wells P11 and P12, the calculated piezometric is close to the measurement, leading to an excellent piezometric fit (Figure 10). In wells P11 and P12, the calculated levels are below those measured. However, the fit can be considered relatively acceptable. This model, under conditions of variable density, in a general way, reproduces the conceptualization of the underground flow in which the eleven wells present hydrodynamic activity due to pumping, causing the aquifer levels to be depressed without recharge due to the absence of rainfall, which means that these levels do not recover in a short time.

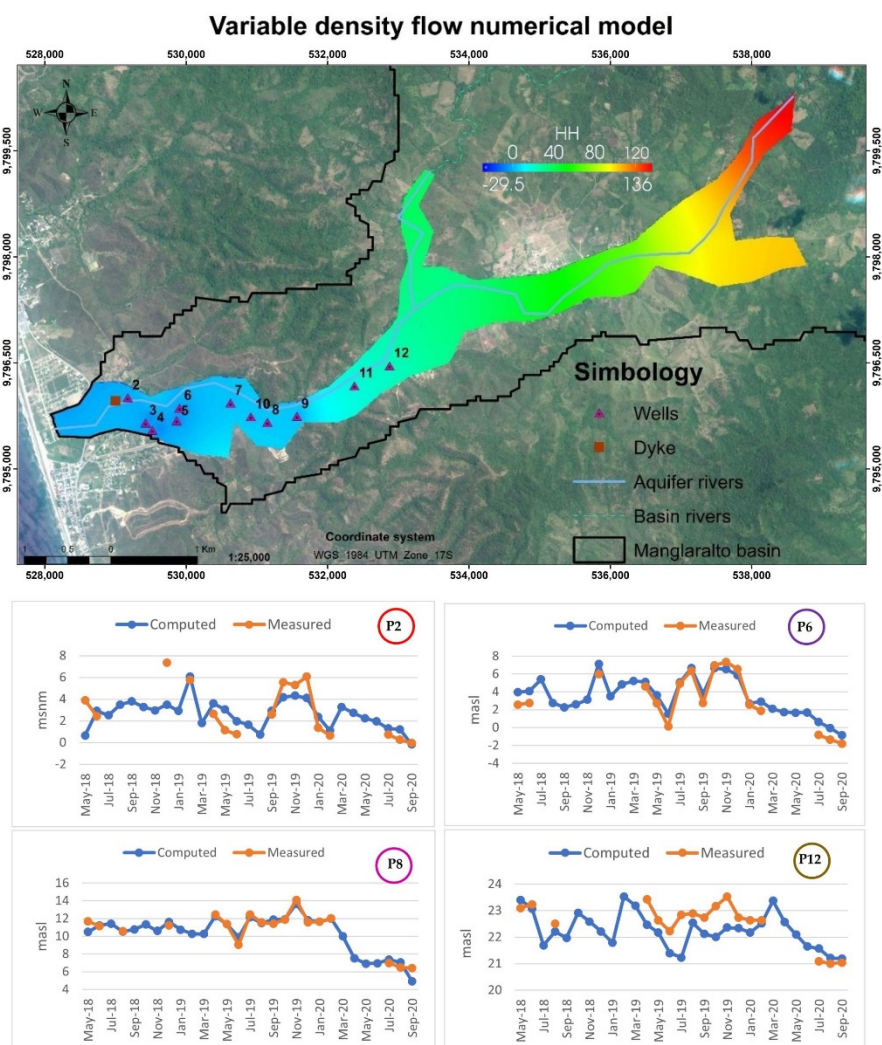


Figure 10. Variable density flow model and hydrograms of wells P2, P6, P8, and P12.

Transport Model

In this model, the variability of the density of the flows present in the basin, which affect the aquifer, is considered, generally presents a good fit (Figure 11), similar to the concentrations calculated in the transport model with constant density. The sources of concentration of the underground flow are the sea and the basement or substrate. Wells P11 and P12 have a higher concentration within the basin; this can occur due to a mixture of recharge water with concentrated water, a product of the substrate's materials. The high variability in well P2 is influenced by its proximity to the shoreline, indicating seawater intrusion. The hydrograms of the flow and transport model of the 11 wells studied in both variable and constant density are in the supplementary material section.

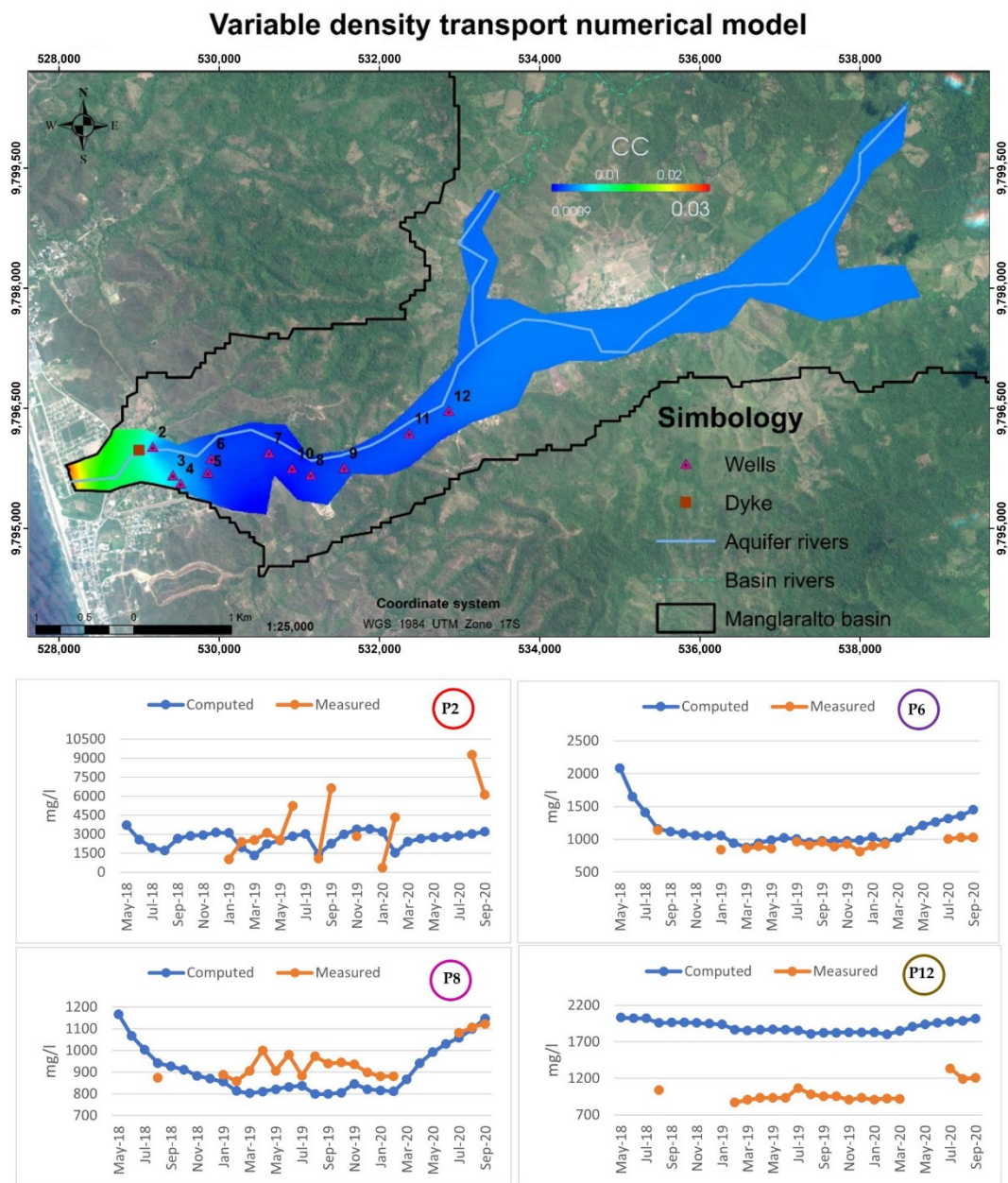
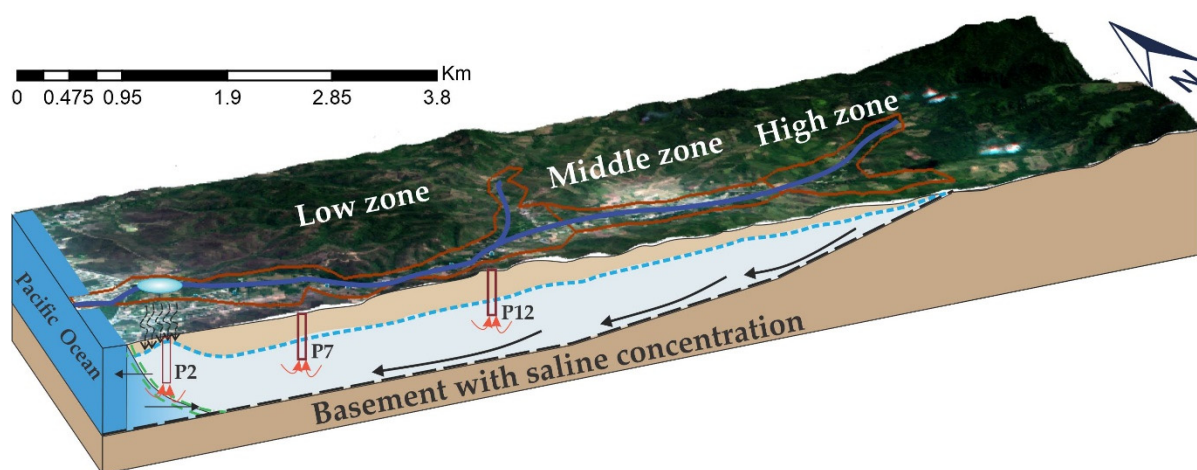


Figure 11. Variable density transport model and hydrograms of wells P2, P6, P8, and P12.

In Figure 12, the system analyzed in this study is synthesized, considering its geographical and hydrogeological parts, visualizing the hydraulic effect of the infiltration produced by the tape near well P2, as well as the advance of marine intrusion into the basin and the importance of the tape in the piezometric concentrations (TDS) water and piezometric levels of the aquifer. The water concentration sources in the basement and the coastal edge by seawater affect groundwater quality for human consumption and supply.



Simbology

- - - Water table
- - - Transition zone (H₂O aquifer-H₂O sea)
- Rivers
- ↕↕ Pumping flow
- Reservoir
- ⊥ Infiltration
- Seawater income
- ← Groundwater discharge
- ⊥ Wells
- Aquifer
- Aquifer edge
- ↔ Flow direction

Figure 12. Schematic synthesis of the Manglaralto coastal aquifer’s hydrogeological system under a satellite image of the study area.

4. Discussion

The hydrograms, both of the constant density flow model and the variable density flow model, obtained from piezometric levels measured in the field and those calculated by Visual Transin 4.0, in general, reproduce the hydrodynamic behavior of the hydrogeological system. The piezometric levels of wells P2, P3, and P4 are influenced by the tape because, in this area, the piezometric levels manage to stay between zero m.a.s.l. and six m.a.s.l. Without this structure, the interval above the levels could not be maintained and would decrease considerably. The tape generates an artificial recharge, which hydraulically causes more significant infiltration to occur, achieving the piezometric levels to increase due to this structure. The closeness or distance of the tape influences the piezometric levels of the water, analogous to what occurs in the numerical model of [57], simulating the effects of artificial recharge in the riverbed, which then infiltrates into the aquifer, increasing the levels in the proximity and forming a barrier against seawater intrusion.

At the points where it is not possible to reproduce the piezometric levels, it is necessary to redefine the parameters of natural recharge and pumping in the wells within the basin, while in the wells near the sea, in addition to these parameters, the hydraulics generated by tape must be reviewed; this is because as the infiltration increases in this area, the piezometric levels’ behavior will depend on the volume in which it infiltrates and periods during which this occurs. The situations are similar to the piezometric levels produced by the effects of different artificial recharge methods around the world presented by [19].

The transport models for constant and variable density show an acceptable adjustment of the concentrations. The wells inside the basin present their concentrations due to the materials that make up the aquifer substrate, which has been subject to regressions and transgressions of the sea towards the continent [38], causing evaporitic materials in the basement, which form a solution in the water. In the aquifer’s lower zone where the study wells are located, the aquifer presents some sustainability, with an approximate

power of 30 m and a saturated thickness of approximately 20 m. However, when the recharge produced by the infiltration of precipitation decreases, the saturated thickness also decreases, leading to the pumping approaching this substrate with higher concentration, producing a mixture with the aquifer water.

In the wells P2, P3, and P4, where the concentration sources are from the sea's substrate, there is evidence that these wells reach high concentrations: mainly P2, which has the highest concentrations in this system (up to 9200 mg/L). The well P12 is at the limit of the lower and middle zones of the Manglaralto river basin (see Figure 2), where the water in the mix (aquifer-basement) has the highest concentration of TDS. Furthermore, the well's depth (approximately 28 m) is very close to the basement with the highest salt concentration. The interior wells present TDS concentrations of up to 1337 mg/L, indicating the mixing of the aquifer water with saline material in the basement. On the other hand, these wells' concentrations decrease considerably in higher rainfall periods (January–May) and the garuas (July–August), which occur throughout the basin. These rain events and the tape facilitate water reservoirs that reinforce the artificial recharge that influences these wells.

The concentrations obtained by the numerical simulation indicate that marine intrusion is present in the basin's interior up to approximately 1 km from the coastline. The transition zone, seawater–groundwater aquifer, is inferred around wells P2, P3, and P4. The advance of seawater intrusion to wells' locations is due to the high pumping periods, a necessary anthropic activity that highlights the communities' development, as indicated [57] and [58], which reinforces the results obtained in the present study. The dry periods related to the decrease in recharge, which is where the importance of the tape becomes evident since, without it, the advance front of the marine intrusion would be found further into the basin, causing these wells to increase their concentration (TDS) and with this decreasing there would be a corresponding decrease in the quality of the water. That this happens is due to the prolonged contribution of infiltration by the reservoir's presence, causing a decrease in concentrations.

5. Conclusions

The numerical model of flow and transport under constant density and variable density shows the tape's hydraulic and environmental importance. The piezometric levels increase considerably in the closest sites in reservoir zones since artificial recharge occurs due to infiltration from the reservoir, causing the levels to predominate for a longer time. With this, the groundwater reduces the concentration (TDS), improving its quality.

The groundwater concentration inside the basin is due to the dissolution of materials present in the substrate, which mix with recharge water from the infiltration of rainfall by pumping effects. The wells closest to the sea have their concentrations due to seawater intrusion and the aquifer substratum. Therefore, in the hydrogeological system, there are two sources of concentration of groundwater.

The numerical simulation shows that marine intrusion is present, and that the advancing front into the basin is approximately in the surroundings of wells P2, P3, and P4. The tape positively impacts the forward front since the recharge is more significant in this area, preventing seawater from entering the basin's interior. Therefore, without this artificial recharge, the concentration would increase towards the other wells. The hydraulic concrete structure has been designed based on the ancestral knowledge, used by the commune members, using artisanal dams, and with the technical–scientific contribution of the academy, it has been possible to design a dam that helps in the storage of surface water and in underground recharge. An added value of the tape located in the area closest to the coastline is seawater intrusion control.

Supplementary Materials: The following are available online at <https://www.mdpi.com/2073-4441/13/4/443/s1>, Figure S1: Well 2 hydrogram (flow model–constant density), Figure S2: Well 3 hydrogram (flow model–constant density), Figure S3: Well 4 hydrogram (flow model–constant density), Figure S4: Well 5 hydrogram (flow model–constant density), Figure S5: Well 6 hydrogram (flow model–constant density), Figure S6: Well 7 hydrogram (flow model–constant density), Figure S7: Well 8 hydrogram (flow model–constant density), Figure S8: Well 9 hydrogram (flow model–constant density), Figure S9: Well 10 hydrogram (flow model–constant density), Figure S10: Well 11 hydrogram (flow model–constant density), Figure S11: Well 12 hydrogram (flow model–constant density), Figure S12: Well 2 hydrogram (transport model–constant density), Figure S13: Well 4 hydrogram (transport model–constant density), Figure S14: Well 4 hydrogram (transport model–constant density), Figure S15: Well 5 hydrogram (transport model–constant density), Figure S16: Well 6 hydrogram (transport model–constant density), Figure S17: Well 7 hydrogram (transport model–constant density), Figure S18: Well 8 hydrogram (transport model–constant density), Figure S19: Well 9 hydrogram (transport model–constant density), Figure S20: Well 10 hydrogram (transport model–constant density), Figure S21: Well 11 hydrogram (transport model–constant density), Figure S22: Well 12 hydrogram (transport model–constant density), Figure S23: Well 2 hydrogram (flow model–variable density), Figure S24: Well 3 hydrogram (flow model–variable density), Figure S25: Well 4 hydrogram (flow model–variable density), Figure S26: Well 5 hydrogram (flow model–variable density), Figure S27: Well 6 hydrogram (flow model–variable density), Figure S28: Well 7 hydrogram (flow model–variable density), Figure S29: Well 8 hydrogram (flow model–variable density), Figure S30: Well 9 hydrogram (flow model–variable density), Figure S31: Well 10 hydrogram (flow model–variable density), Figure S32: Well 11 hydrogram (flow model–variable density), Figure S33: Well 12 hydrogram (flow model–variable density), Figure S34: Well 2 hydrogram (transport model–variable density), Figure S35: Well 3 hydrogram (transport model–variable density), Figure S36: Well 4 hydrogram (transport model–variable density), Figure S37: Well 5 hydrogram (transport model–variable density), Figure S38: Well 6 hydrogram (transport model–variable density), Figure S39: Well 7 hydrogram (transport model–variable density), Figure S40: Well 8 hydrogram (transport model–variable density), Figure S41: Well 9 hydrogram (transport model–variable density), Figure S42: Well 10 hydrogram (transport model–variable density), Figure S43: Well 11 hydrogram (transport model–variable density), Figure S44: Well 12 hydrogram (transport model–variable density), Table S1: Monthly data on precipitation and values obtained in recharge and PET, Table S2: Annual data of precipitation and values obtained in recharge and PET.

Author Contributions: Conceptualization, P.C.-M., F.J.M., F.M.-C., C.L.-F.d.V., and B.A.-M.; methodology, F.J.M., F.M.-C., C.L.-F.d.V., and B.A.-M.; software, J.H., C.L.-F.d.V., and B.A.-M.; validation, F.J.M., J.H., C.L.-F.d.V., and B.A.-M.; formal analysis, P.C.-M., F.J.M., F.M.-C., C.L.-F.d.V., and B.A.-M.; investigation, P.C.-M., F.J.M., F.M.-C., C.L.-F.d.V., and B.A.-M.; resources, P.C.-M. and F.M.-C.; data curation, F.J.M., C.L.-F.d.V., B.A.-M., and F.M.-C.; writing—original draft preparation, C.L.-F.d.V., and B.A.-M.; writing—review and editing, P.C.-M., F.J.M., F.M.-C., and J.H.; visualization, C.L.-F.d.V., and B.A.-M.; supervision, P.C.-M., F.J.M., and F.M.-C.; project administration, P.C.-M., F.J.M., and F.M.-C.; funding acquisition, P.C.-M., and F.J.M. All authors have read and agreed to the published version of the manuscript.

Funding: The ESPOL Social Link Project funded this research: “Resilience in water management, in the face of COVID-19, Manglaralto”. CODE: PG03-PY20-03 and the IAEA Project: “Improvement of coastal aquifers’ management by studying the recharge rate of the alluvial aquifer of the Manglaralto river basin”. CODE: ECU/7/005.

Institutional Review Board Statement: Not applicable.

Informed Consent Statement: Not applicable.

Data Availability Statement: Not applicable.

Acknowledgments: The authors want to thank the members of the JAAPMAN Water Board, especially the president, Rocío Muñoz, for the ESPOL Project: “Register of geological and mining heritage and its incidence in the defence and preservation of geodiversity in Ecuador”. CODE: CIPAT-01-2018, and the UPSE project: “Geophysical and hydrochemical characterization of the Manglaralto aquifer for the sustainability of the water resource”. CODE: 91870000.0000.382444.

Conflicts of Interest: The authors declare no conflict of interest.

References

1. USGS. Water Science Basics. Available online: http://www.nysenvirothon.org/Referencesandother/Water_Science_Basics.pdf (accessed on 30 November 2020).
2. Astrálaga, M. La Convención Ramsar y los ecosistemas de Manglar. *Secr. Conv. Ramsar*. **2006**, 1–6. Available online: https://barqueroweb.synthasite.com/resources/SRN_I/Astr%C3%A1laga%202006.pdf (accessed on 30 November 2020).
3. Astrálaga, M. La Convención sobre los Humedales Ramsar. *Trop. J. Environ. Sci.* **2001**, *21*, 23–29. [[CrossRef](#)]
4. Erwin, K.L. Wetlands and global climate change: The role of wetland restoration in a changing world. *Wetl. Ecol. Manag.* **2008**, *17*, 71–84. [[CrossRef](#)]
5. Zedler, J.B.; Kercher, S.; Davidson, N.C. Wetland resources: Status, trends, ecosystem services, and restorability. *Mar. Freshw. Res.* **2014**, *65*, 934–941. [[CrossRef](#)]
6. Valsero, D.J.J.; De Domingo, G.A.; Ardila, R.P. Propuesta de clasificación genético-geológica de humedales. Aplicación a los humedales españoles incluidos en el convenio de Ramsar. *Bol. Geol. Min.* **2009**, *120*, 335–346.
7. Arias-García, J.; Gómez-Zotano, J. La planificación y gestión de los humedales de Andalucía en el marco del Convenio Ramsar. *Investig. Geográficas* **2015**, *120*, 117. [[CrossRef](#)]
8. Herrera, G.; Alavarado-Macancela, N.; Gavín-Quinchuela, T.; Carrión, P. Puesta en valor del sistema río-acuífero costero manglaralto en el contexto del proyecto geoparque ancón-santa elena: Motor de desarrollo en áreas rurales de la parroquia manglaralto, ecuador. *Proc. LACCEI Int. Multi-Conf. Eng. Educ. Technol.* **2019**, 2019. [[CrossRef](#)]
9. Da Silva, G.C.; Bocanegra, E.; Custodio, E.; Manzano, M.; Montenegro, S. State of knowledge and management of Iberoamerican coastal aquifers with different geo-hydrological settings. *Episodes* **2010**, *33*, 91–101. [[CrossRef](#)]
10. Ferguson, G.; Gleeson, T. Vulnerability of coastal aquifers to groundwater use and climate change. *Nat. Clim. Chang.* **2012**, *2*, 342–345. [[CrossRef](#)]
11. Gleeson, T.; Wada, Y.; Bierkens, M.F.P.; Van Beek, L.P.H. Water balance of global aquifers revealed by groundwater footprint. *Nature* **2012**, *488*, 197–200. [[CrossRef](#)]
12. Kinniburgh, D.G.; Gale, I.N.; Smedley, P.L.; Darling, W.G.; West, J.M.; Aldous, P.J.; O’Shea, M.J. The effects of historic abstraction of groundwater from the London Basin aquifers on groundwater quality. *Appl. Geochem.* **1994**, *9*, 175–195. [[CrossRef](#)]
13. Datta, P.S.; Bhattacharya, S.K.; Tyagi, S.K. 18O studies on recharge of phreatic aquifers and groundwater flow-paths of mixing in the Delhi area. *J. Hydrol.* **1996**, *176*, 25–36. [[CrossRef](#)]
14. Martínez, D.E.; Bocanegra, E.M. Hydrogeochemistry and cation-exchange processes in the coastal aquifer of Mar Del Plata, Argentina. *Hydrogeol. J.* **2002**, *10*, 393–408. [[CrossRef](#)]
15. Pool, M.; Carrera, J.; Alcolea, A.; Bocanegra, E.M. A comparison of deterministic and stochastic approaches for regional scale inverse modeling on the Mar del Plata aquifer. *J. Hydrol.* **2015**, *531*, 214–229. [[CrossRef](#)]
16. Wada, Y.; Van Beek, L.P.H.; Van Kempen, C.M.; Reckman, J.W.T.M.; Vasak, S.; Bierkens, M.F.P. Global depletion of groundwater resources. *Geophys. Res. Lett.* **2010**, *37*. [[CrossRef](#)]
17. Hani, A.; Lallahem, S.; Mania, J.; Djabri, L. On the use of finite-difference and neural-network models to evaluate the impact of underground water overexploitation. *Hydrol. Process.* **2006**, *20*, 4381–4390. [[CrossRef](#)]
18. Carrión, P.; Herrera, G.; Briones, J.; Sánchez, C.; Limón, J. Practical adaptations of ancestral knowledge for groundwater artificial recharge management of Manglaralto coastal aquifer, Ecuador. *WIT Trans. Ecol. Environ.* **2018**, *217*, 375–386. [[CrossRef](#)]
19. Bouwer, H. Artificial recharge of groundwater: Hydrogeology and engineering. *Hydrogeol. J.* **2002**, *10*, 121–142. [[CrossRef](#)]
20. Voss, C.; Souza, W. Variable density flow and solute transport simulation of regional aquifers containing a narrow freshwater-saltwater transition zone. *Water Resour.* **1987**, *23*, 1851–1866. [[CrossRef](#)]
21. Tweed, S.O.; Weaver, T.R.; Cartwright, I. Distinguishing groundwater flow paths in different fractured-rock aquifers using groundwater chemistry: Dandenong Ranges, southeast Australia. *Hydrogeol. J.* **2005**, *13*, 771–786. [[CrossRef](#)]
22. Shu, L.; Zou, Z.; Li, F.; Wu, P.; Chen, H.; Xu, Z. Laboratory and numerical simulations of spatio-temporal variability of water exchange between the fissures and conduits in a karstic aquifer. *J. Hydrol.* **2020**, *590*, 125219. [[CrossRef](#)]
23. Song, K.; Ren, X.; Mohamed, A.K.; Liu, J.; Wang, F. Research on drinking-groundwater source safety management based on numerical simulation. *Sci. Rep.* **2020**, *10*, 1–17. [[CrossRef](#)]
24. Huyakorn, P.S.; Andersen, P.F.; Mercer, J.W.; White, H.O. Saltwater intrusion in aquifers: Development and testing of a three-dimensional finite element model. *Water Resour. Res.* **1987**, *23*, 293–312. [[CrossRef](#)]
25. Werner, A.D.; Bakker, M.; Post, V.E.A.; Vandenbohede, A.; Lu, C.; Ataie-Ashtiani, B.; Simmons, C.T.; Barry, D.A. Seawater intrusion processes, investigation and management: Recent advances and future challenges. *Adv. Water Resour.* **2013**, *51*, 3–26. [[CrossRef](#)]
26. Lathashri, U.A.; Mahesha, A. Simulation of saltwater intrusion in a coastal aquifer in Karnataka, India. *Aquat. Procedia* **2015**, *4*, 700–705. [[CrossRef](#)]
27. Santos, M.R.P.; Santiago, M.M.F.; Mendonça, L.A.R.; Frischkorn, H.; Filho, J.M. Modelagem do transporte de cloreto proveniente de esgoto urbano em um aquífero sedimentar usando MT3D: O caso da bateria de poços de Juazeiro do Norte (CE). *Eng. Sanit. Ambient.* **2014**, *19*, 283–292. [[CrossRef](#)]
28. Hirata, R.; Cagnon, F.; Bernice, A.; Maldaner, C.H.; Galvão, P.; Marques, C.; Terada, R.; Varnier, C.; Ryan, M.C.; Bertolo, R. Nitrate contamination in brazilian urban aquifers: A tenacious problem. *Water* **2020**, *12*, 2709. [[CrossRef](#)]
29. Tojeda, I.; Cienfuegos, R.; Muñoz, J.; Durán, M. Numerical modeling of saline intrusion in Salar de Atacama. *J. Hydrol. Eng.* **2003**, 25–34. [[CrossRef](#)]

30. Vásquez, C.; Ortiz, C.; Suárez, F.; Muñoz, J.F. Modeling flow and reactive transport to explain mineral zoning in the Atacama salt flat aquifer, Chile. *J. Hydrol.* **2013**, *490*, 114–125. [[CrossRef](#)]
31. Hugman, R.; Stigter, T.; Costa, L.; Monteiro, J.P. Numerical modelling assessment of climate-change impacts and mitigation measures on the Querença-Silves coastal aquifer (Algarve, Portugal). *Hydrogeol. J.* **2017**, *25*, 2105–2121. [[CrossRef](#)]
32. Datta, B.; Vennalakanti, H.; Dhar, A. Modeling and control of saltwater intrusion in a coastal aquifer of Andhra Pradesh, India. *J. Hydro-Environ. Res.* **2009**, *3*, 148–159. [[CrossRef](#)]
33. Mascioli, S.; Benavente, M.; Martínez, D.E. Estimation of transport hydraulic parameters in loessic sediment, Argentina: Application of column tests. *Hydrogeol. J.* **2005**, *13*, 849–857. [[CrossRef](#)]
34. Xu, Z.; Hu, B.X.; Xu, Z.; Wu, X. Simulating seawater intrusion in a complex coastal karst aquifer using an improved variable-density flow and solute transport—Conduit flow process model. *Hydrogeol. J.* **2019**, *53*. [[CrossRef](#)]
35. Jinno, K.; Tsutsumi, A.; Hiroshiro, Y. Three dimensional solute transport numerical modeling of salinity fluctuations in a coastal aquifer. In Proceedings of the 18th World IMACS Congress and MODSIM09 International Congress on Modelling and Simulation, Cairns, Australia, 13–17 July 2009; pp. 4128–4134.
36. Herrera-Franco, G.; Carrión-Mero, P.; Alvarado, N.; Morante-Carballo, F.; Maldonado, A.; Caldevilla, P.; Briones-Bitar, J.; Berrezueta, E. Geosites and georesources to foster geotourism in communities: Case study of the santa elena peninsula geopark project in ecuador. *Sustainability* **2020**, *12*, 4484. [[CrossRef](#)]
37. El Universo Problemas en Manglaralto. Available online: www.eluniverso.com/opinion/2015/10/19/nota/5192870/problemas-manglaralto (accessed on 30 November 2020).
38. Morante, F.; Montalván, F.J.; Carrión, P.; Herrera, G.; Heredia, J.; Elorza, F.J.; Pilco, D.; Solórzano, J. Hydrochemical and geological correlation to establish the groundwater salinity of the coastal aquifer of the Manglaralto River basin, Ecuador. *WIT Trans. Ecol. Environ.* **2019**, *229*, 139–149. [[CrossRef](#)]
39. Herrera-Franco, G. Estudio Para Un Modelo de Gestión de Un Acuífero Costero, Mediante Metodologías Participativas y Análisis Geoestadístico en El Marco Del Desarrollo Local. Manglaralto, Ecuador. Doctoral Dissertation, Universidad Politécnica de Madrid, Madrid, Spain, 2015.
40. Gricelda, H.F.; Paúl, C.M.; Niurka, A.M. Participatory process for local development: Sustainability of water resources in rural communities: Case manglaralto-santa elena, ecuador. *World Sustain. Ser.* **2018**, 663–676. [[CrossRef](#)]
41. Franco, G.H.; Quinchuelaa, T.G.; Macancela, N.A.; Mero, P.C. Participative analysis of socio-ecological dynamics and interactions. A case study of the Manglaralto Coastal Aquifer, Santa Elena-Ecuador. *Malays. J. Sustain. Agric.* **2017**, *1*, 19–22. [[CrossRef](#)]
42. Carballo, F.M.; Brito, L.M.; Mero, P.C.; Aguilar, M.A.; Ramírez, J.T. Urban wastewater treatment through a system of green filters in the Montañita commune, Santa elena, Ecuador. *WIT Trans. Ecol. Environ.* **2019**, *239*, 233–249. [[CrossRef](#)]
43. Thiel, M.; Macaya, E.C.; Acuña, E.; Arntz, W.E.; Bastias, H.; Brokordt, K.; Camus, P.A.; Castilla, J.C.; Castro, L.R.; Cortés, M.; et al. The humboldt current system of northern and central chile oceanographic processes, ecological interactions and socioeconomic feedback. *Oceanogr. Mar. Biol.* **2007**, *45*, 195–344.
44. Montecino, V.; Lange, C.B. The Humboldt Current System: Ecosystem components and processes, fisheries, and sediment studies. *Prog. Oceanogr.* **2009**, *83*, 65–79. [[CrossRef](#)]
45. Peel, M.C.; Finlayson, B.L.; McMahon, T.A. Updated world map of the Köppen-Geiger climate classification. *Hydrol. Earth Syst. Sci.* **2007**, *11*, 1633–1644. [[CrossRef](#)]
46. Herrera-Franco, G.; Carrión-Mero, P.; Aguilar-Aguilar, M.; Morante-Carballo, F.; Jaya-Montalvo, M.; Morillo-Balsera, M.C. Groundwater resilience assessment in a communal coastal aquifer system. The case of Manglaralto in Santa Elena, Ecuador. *Sustainability* **2020**, *19*, 8290. [[CrossRef](#)]
47. Herrera Franco, G.; Flores Ruíz, D.; Herrera Franco, D.; Flores Ruiz, G. Aspectos socioeconómicos de la gestión del agua y el turismo en las comunas Olón y Manglaralto de la provincia de Santa Elena (Ecuador). In *Cooperación Transfronteriza Andalucía-Algarve-Alentejo*; Universidad de Huelva: Huelva, Spain, 2009; pp. 250–252.
48. Groundwater Hydrology Group Visual Transin. Available online: <https://h2ogeo.upc.edu/en/investigation-hydrogeology/software/152-visual-transin-en> (accessed on 30 November 2020).
49. Heredia, J.; Murillo Díaz, J.M. Estado del arte sobre la representación numérica de sistemas de flujo bajo condiciones de densidad variable. *Bol. Geol. Min.* **2007**, *118*, 555–576.
50. Franco, H.G.; Mero, C.P.; Bitar, B.J. Management practices for a sustainable community and its impact on development, Manglaralto-Santa elena, Ecuador. *Proc. LACCEI Int. Multi-Conf. Eng. Educ. Technol.* **2019**, *2019*, 24–26. [[CrossRef](#)]
51. Nuñez del Arco, E. *Geología del Ecuador*; Escuela Superior Politécnica del Litoral: Guayaquil, Ecuador, 2003.
52. Ávila-Dávila, L.; Soler-Méndez, M.; Madrona-Sánchez, P.; Ruiz-Canales, A.; Bautista-Capetillo, C.F.; González-Trinidad, J.; Molina-Martínez, J.M. Análisis de la velocidad de infiltración del agua en el suelo saturados mediante lisímetros de pesada. 2019, pp. 642–648. Available online: <https://zaguan.unizar.es/record/84426?ln=en> (accessed on 30 November 2020). [[CrossRef](#)]
53. Ojeda, A.; Mc Leod, C.; Águila, K.; Pino, M.T. Bases para la determinación de las necesidades hídricas del cultivo del calafate in situ, para su adaptación al manejo agronómico. *Inf. INIA Kampenaike* **2018**, *79*, 1–6. Available online: <https://biblioteca.inia.cl/handle/123456789/4880> (accessed on 30 November 2020).
54. Toala, J.M.F.; Quinde, M.C.M.; Gómez, G.R. Hydrological modeling of the manglaralto river for the generation of flood maps (Santa Elena-Ecuador). *Proc. LACCEI Int. Multi-Conf. Eng. Educ. Technol.* **2020**, 27–31. [[CrossRef](#)]

-
55. Catuto, M. Modelación Hidrológica del río Manglaralto para la Generación de Mapas de Inundación de la Parroquia Manglaralto Provincia de Santa Elena. Bachelor's Thesis, Universidad Estatal Península de Santa Elena, Santa Elena, Ecuador, 2020.
 56. Sanchez, J. Evapotranspiración. *Univ. Salamanca* **2015**, *1*, 1–9.
 57. Motallebian, M.; Ahmadi, H.; Raoof, A.; Cartwright, N. An alternative approach to control saltwater intrusion in coastal aquifers using a freshwater surface recharge canal. *J. Contam. Hydrol.* **2019**, *222*, 56–64. [[CrossRef](#)]
 58. Lèye, B.; Koko, J.; Kane, S.; Sy, M. Numerical simulation of saltwater intrusion in coastal aquifers with anisotropic mesh adaptation. *Math. Comput. Simul.* **2018**, *154*, 1–18. [[CrossRef](#)]